

Article

# Adsorption of Methylene Blue in Water onto Activated Carbon by Surfactant Modification

Yu Kuang <sup>1</sup> , Xiaoping Zhang <sup>1,2,3,4,\*</sup> and Shaoqi Zhou <sup>1</sup>

<sup>1</sup> School of Environment & Energy, Guangzhou Higher Education Mega Centre, South China University of Technology, Guangzhou 510006, China; eskuangyu@mail.scut.edu.cn (Y.K.); fesqzhou@yeah.net (S.Z.)

<sup>2</sup> The Key Laboratory of Pollution Control and Ecosystem Restoration in Industry Clusters of Ministry of Education, Guangzhou 510006, China

<sup>3</sup> Guangdong Environmental Protection Key Laboratory of Solid Waste Treatment and Recycling, Guangzhou 510006, China

<sup>4</sup> Guangdong Provincial Engineering and Technology Research Center for Environmental Risk Prevention and Emergency Disposal, Guangzhou 510006, China

\* Correspondence: xpzhang@scut.edu.cn; Tel.: +86-1367-892-0429

Received: 19 January 2020; Accepted: 18 February 2020; Published: 21 February 2020



**Abstract:** In this paper, the enhanced adsorption of methylene blue (MB) dye ion on the activated carbon (AC) modified by three surfactants in aqueous solution was researched. Anionic surfactants—sodium lauryl sulfate (SLS) and sodium dodecyl sulfonate (SDS)—and cationic surfactant—hexadecyl trimethyl ammonium bromide (CTAB)—were used for the modification of AC. This work showed that the adsorption performance of cationic dye by activated carbon modified by anionic surfactants (SLS) was significantly improved, whereas the adsorption performance of cationic dye by activated carbon modified by cationic surfactant (CTAB) was reduced. In addition, the effects of initial MB concentration, AC dosage, pH, reaction time, temperature, real water samples, and additive salts on the adsorption were studied. When  $\text{Na}^+$ ,  $\text{K}^+$ ,  $\text{Ca}^{2+}$ ,  $\text{NH}_4^+$ , and  $\text{Mg}^{2+}$  were present in the MB dye solution, the effect of these cations was negligible on the adsorption (<5%). The presence of  $\text{NO}_2^-$  improved the adsorption performance significantly, whereas the removal rate of MB was reduced in the presence of competitive cation ( $\text{Fe}^{2+}$ ). It was found that the isotherm data had a good correlation with the Langmuir isotherm through analyzing the experimental data by various models. The dynamics of adsorption were better described by the pseudo-second-order model and the adsorption process was endothermic and spontaneous. The results showed that AC modified by anionic surfactant was effective for the adsorption of MB dye in both modeling water and real water.

**Keywords:** activated carbon; modification; surfactant; adsorption; methylene blue; ions effect

## 1. Introduction

As a cationic dye, methylene blue ( $\text{C}_{16}\text{H}_{18}\text{ClN}_3\text{S}$ , MB) is widely used in chemical indicators, dyes and biological dyes. A large amount of organic dye wastewater is produced in the processes of the printing and dyeing industries. The dye wastewater has characteristics such as large discharge, high chromaticity, high organic matter concentration, and poor biodegradability, and greatly affects the water body health and the photosynthesis of microorganisms in the water environment [1,2].

At present, many researchers have used different methods to treat the dye wastewater [3]. Typical treatment methods include physical, chemical, and biological methods, such as flocculation [4], membrane filtration [5,6], advanced oxidation [7], ozonation, photocatalytic degradation [8], and biodegradation. These traditional methods have inherent limitations [9] such as the complex and uneconomical of nature of the technology, and thus it is necessary to seek efficient and simple dye wastewater treatment methods [10].

Compared with other treatment methods, the adsorption method is considered as prevailing over other dye wastewater treatment technology due to its advantages such as high efficiency, low cost, simple operation, and insensitive of toxic substances [11]. Activated carbon is the most commonly used adsorbent, and is widely used to remove the organic and inorganic pollutants in water phase.

Adsorption capacity is an important index to evaluate the adsorption effect of adsorbent. Various low-cost alternative adsorbents from agricultural solid waste, industrial solid waste, agricultural by-products, and biomass are used in wastewater treatment. For example, clay [12], sludge [13], montmorillonite [14], flax fiber [15], zeolite [16,17], and biochar (rice husk [18,19], pinewood [20], wheat [21], sugarcane bagasse [22], switchgrass [23], *Ficus carica* bast [24]) as adsorbents have been used for adsorption treatment of dye wastewater. However, common activated carbon is not widely used to adsorb and remove pollutants due to its low adsorption capacity, which is caused by small specific surface area and poor adsorption selection performance, as well as limitations of the surface functional groups and electrochemical properties.

In many cases, it is required to modify activated carbon surface to enhance its affinity with target pollutants and increase its adsorption capacity and improve the removal effect of pollutants in different types of industrial wastewater. The methods used to modify activated carbon include physical, chemical, and biological methods. As a chemical modification technology of activated carbon, surfactant modification shows great significance. Surfactant modification for activated carbon can improve the hydrophilicity and the dispersion of activated carbon in water due to an increase in the affinity between activated carbon and water and the decrease of the attractive energy between particles. Surfactant has the advantages of low cost [25] and less damage to the structure of activated carbon. Moreover, the surfactant can change the surface charge characteristics of activated carbon and provide more ionic adsorption sites for pollutants, which can not only enhance the adsorption capacity of ionic pollutants on activated carbon [26], but also can promote selective adsorption.

In wastewater treatment, activated carbon modified by surfactant is used as an adsorbent to remove various pollutants, including organic pollutants [26,27], reactive dyes [15,21,28,29], and heavy metals [30,31]. Surfactants are classified into anionic, cationic, non-ionic, and amphoteric ions according to the type and performance of the hydrophilic group [22]. Sodium lauryl sulfate (SLS) is a nontoxic anionic surfactant. Much research into the effect on inorganic metal ions by activated carbon modified by surfactant has been reported, however, the study of organic dyes adsorption by SLS-C has been rarely reported.

Previous research has shown that activated carbon modified by different surfactants have different effects on various water quality dye wastewater. Therefore, it is necessary to determine how the coexistence of other ions would affect the adsorption. Meanwhile, more information is still required in order to better understand of the adsorption behavior of methylene blue cationic dyes on modified-activated carbon.

The feasibility of removing MB from aqueous solution by surfactant-modified activated carbon was investigated. The purposes of the study were to (1) confirm the adsorption rate and capacity through the adsorption models; (2) determine the various parameters that affect sorption, such as initial dye concentration, temperature, pH, adsorbent dose, and additive salts; and (3) obtain the adsorption effect of adsorbent in actual water samples.

## 2. Materials and Methods

### 2.1. Materials

Methylene blue (Figure 1,  $C_{16}H_{18}ClN_3S$ ) was used as adsorbent. The molar mass of MB molecule is  $319.85 \text{ g}\cdot\text{mol}^{-1}$ . The surfactants used in this study were sodium lauryl sulfate (SLS,  $C_{12}H_{25}SO_4Na$ ), sodium dodecyl sulfonate (SDS,  $C_{12}H_{25}SO_3Na$ ), and hexadecyl trimethyl ammonium bromide (CTAB). Other chemicals used were calcium chloride ( $CaCl_2$ ), magnesium sulfate heptahydrate ( $MgSO_4\cdot 7H_2O$ ), sodium sulfate ( $Na_2SO_4$ ), potassium chloride (KCl), sodium chloride (NaCl), sodium nitrite ( $NaNO_2$ )

and ferrous sulfate ( $\text{FeSO}_4$ ). All chemicals were purchased from Shanghai Aladdin Bio-Chem Technology Co., LTD. The powdered activated carbon (AC) was purchased from Tianjin Fuchen Chemical Reagent Co., Ltd. All the chemicals were used without any further purification.

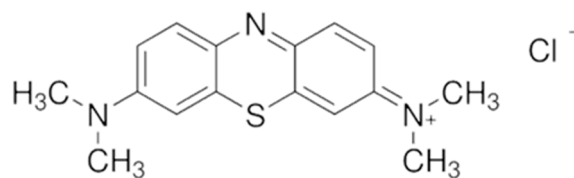


**Figure 1.** The chemical structure of methylene blue (MB).

### 2.2. Preparation of Surfactant-modified Activated Carbon

A total of 5 g of AC and 8.60 mM anionic surfactant SLS were added to 100 mL of solution. The mixture was oscillated in a shaker at 301 K for 6 h, and after that, the AC was filtrated and washed with deionized water. The filtrated AC was dried in an air-dry oven at 313 K for 24 h, and then was stored in a sealed and dry environment. Studies have shown that the concentration of surfactant corresponding to critical micelle concentration (CMC) is the best for adsorption [32]. It has been reported that the critical micelle concentration (CMC) of SLS is 8.60 mM at 28°C. The raw AC and surfactant-modified AC were called Virgin-C and SLS-C, respectively. The surfactant sodium dodecyl sulfonate (SDS) and hexadecyl trimethyl ammonium bromide (CTAB) were used to modify AC in the same method at the concentration of 1 CMC, called SDS-C and CTAB-C, respectively.

### 2.3. Adsorption Experiments

The adsorption capacity of MB on modified AC carried out in the batch adsorption experiment by investigating the effect of experimental variables such as pH (1–12), initial MB concentration (10, 30, 50  $\text{mg}\cdot\text{L}^{-1}$ ), contact time, adsorbent dosage, temperature (298, 308, 318, 328K), and ionic species. The initial pH of the solution was adjusted with 0.1 M hydrochloric acid (HCl) and sodium hydroxide (NaOH) solution and determined with pH meter. A certain amount of modified AC was added to a 250 mL conical flask solution containing 100 mL of solution at certain concentrations of MB. Each mixture was oscillated at 170  $\text{r}\cdot\text{min}^{-1}$  at 25 °C at the given time interval. After the adsorption process, the samples were filtered and analyzed. The reserve solution of MB (1  $\text{g}\cdot\text{L}^{-1}$ ) was prepared by dissolving the suitable amount MB in distilled water. All the experiments were done in triplicate.

### 2.4. Analytical Methods

According to the Standard Methods of Water and Wastewater Monitoring and Analysis Method, the absorbance of MB solution was measured by UV-visible spectrophotometer (INESA Scientific Instrument Co., Ltd. Shanghai, China) at 664 nm, which is the maximum absorption peak of MB. The concentration and removal rate of MB was obtained through the curve of relationship between solution concentration and absorbance of MB (Figure S1). The pH was measured using a DZS-706A multi-parameter meter (INESA Scientific Instrument Co., Ltd. Shanghai, China).

By measuring the absorbance of dye solution before and after treatment, the removal of MB on SLS-C adsorbent was studied with the batch equilibrium method. On the basis of Equations (1) and (2), the removal rate of dye in equilibrium state was calculated.

$$Q_e = \frac{(C_0 - C_e)V}{m} \quad (1)$$

$$\text{Removal percentage} = \frac{(C_0 - C_e)}{C_0} \times 100, \quad (2)$$

where  $Q_e$  represents the quantity of dye per unit mass of adsorbent ( $\text{mg}\cdot\text{g}^{-1}$ );  $C_0$  and  $C_e$  are the initial and equilibrium concentrations, respectively;  $V$  is the volume of MB dye solution in liters; and  $m$  is the weight of SLS-C adsorbent in grams.

### 3. Results

#### 3.1. Effect of Different Surfactants

Figure 2 showed the extent of adsorption of MB on AC modified with different surfactants in aqueous solution at the initial MB concentration of  $50 \text{ mg}\cdot\text{L}^{-1}$ . The results showed that SLS-C represents the highest MB adsorption capacity, followed by Virgin-C, SDS-C, and CTAB-C.

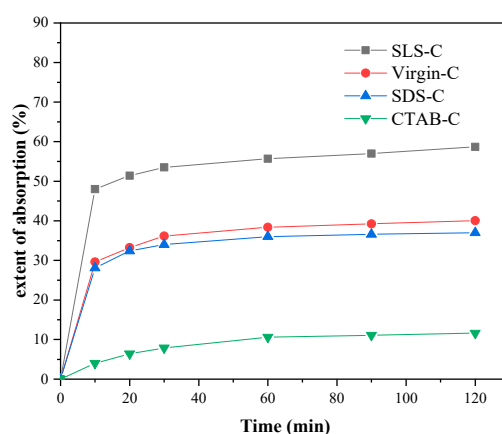


**Figure 2.** MB removal by using different activated carbons (ACs) (initial MB concentration =  $50 \text{ mg}\cdot\text{L}^{-1}$ ,  $S/L = 0.15 \text{ g}\cdot\text{L}^{-1}$ ,  $T = 298 \text{ K}$ ,  $\text{pH} = 5.0$ ).

Compared with SLS-C and SDS-C, CTAB-C showed the weakest adsorption for MB dye. As a cationic surfactant, CTAB had a repulsive force with dye cations and occupied the adsorption sites on activated carbon, resulting in a low adsorption capacity of cationic MB dye.

Compared with the unmodified AC, surfactants loaded on activated carbon may clog the pores of AC, which reduces its ability to adsorb MB. On the other hand, the ionic functional groups of loaded surfactants can provide ion exchange sites with a higher affinity for MB than the unmodified AC surface. The higher MB adsorption on SLS-C compared with Virgin-C indicated that the positive effect of the functional group of SLS-C exceeded the negative effect of the pore blocking, whereas the lower MB removal by SDS-C compared with Virgin-C indicated that the negative effect of the pore blocking exceeded the positive effect of the functional group of SDS-C.

AC modified by anionic surfactants showed a strong adsorption capacity for MB dye due to the strong binding between the anionic surfactant and the cationic MB dye. The chemical properties of the functional groups of surfactant play an important role in adsorption. The cations attached to the strong acid conjugate base of SLS, such as sodium ions (e.g.,  $\text{R-SO}_3^- \text{Na}^+$ ) and protons (e.g.,  $\text{R-SO}_3^- \text{H}^+$ ), can be easily dissociated in aqueous solution and exchanged with an MB ion [27]. Therefore the SLS-C showed high MB removal effect. The affinity between the functional group on SDS and MB dye was weaker than that of SLS due to it being without strong acid conjugate base, which made the adsorption effect on MB lower than SLS-C.

The possible chemical adsorption processes of MB on SLS-C are shown in Figure 3. The reactions between MB dye cation ( $\text{M}^+$ ) with  $\text{RSO}_3\text{Na}$  on SLS-C occurred regarding Equations (3)–(5).  $\text{RSO}_3\text{Na}$  is the active hydrophilic group of SLS and  $\text{ROH}$  represents the carboxyl, phenolic hydroxyl on AC.



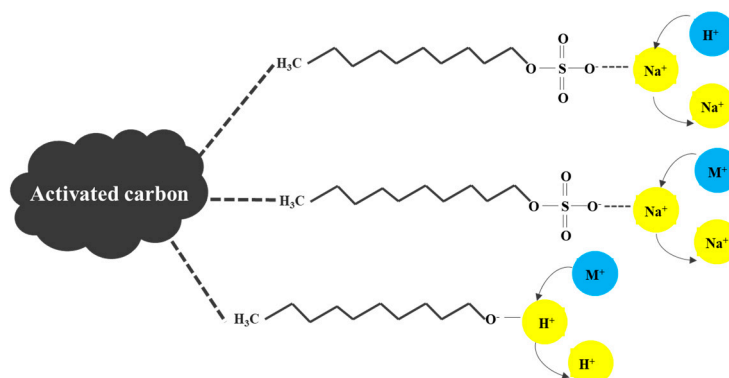
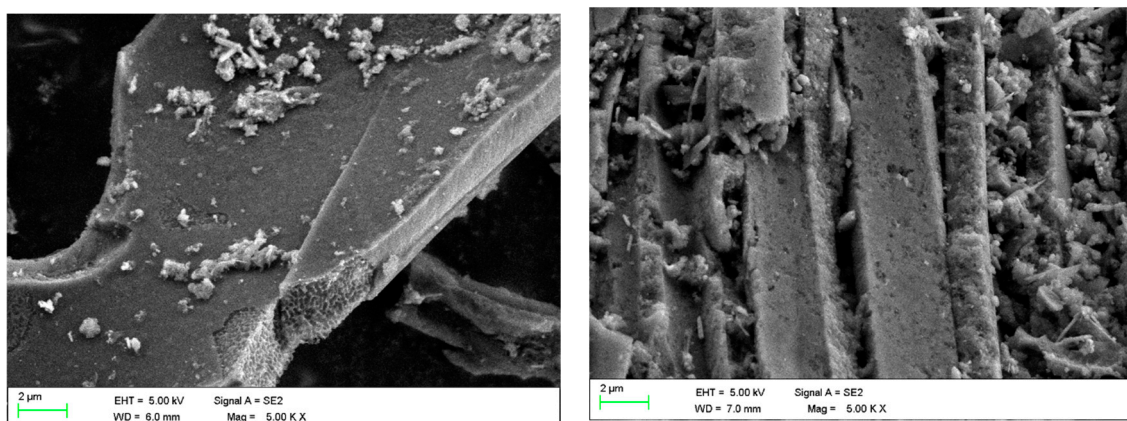


**Figure 3.** The chemical adsorption between MB dye and the surface functional groups on sodium lauryl sulfate (SLS)-C.

### 3.2. Characterization of SLS-C

FE-SEM (Field Emission Scanning Electron Microscope) was used to observe the surface of the adsorbent. Figure 4 shows the detailed surface characteristics of the adsorbent. Figure 4a shows the surface of Virgin-C with a small amount of carbon debris and micropore of different sizes. Figure 4b shows the surface of SLS-C with a great quantity of pores and a large number of material debris occupying the pores compared with untreated AC. This was due to the electrostatic interaction and adhesion of SLS molecules. A large number of material debris occupied the pores, which could lead to a reduction in surface area, but could provide adsorption and ion exchange sites for MB.



(a) FE-SEM-image of Virgin-C

(b) FE-SEM-image of SLS-C

**Figure 4.** FE-SEM pictures of (a) Virgin-C and (b) SLS-C.

### 3.3. Effects of Initial Solution pH

Figure 5 shows the variation of removal rate and adsorption capacities of MB on SLS-C at various pH values. As can be seen from Figure 5a, the alkaline condition was favorable for the adsorption of MB on SLS-C. According to Figure 5b, when the initial concentration of MB was 10, 30, and 50 mg·L<sup>-1</sup>, the adsorption capacities of MB were 62.67, 168.39, and 193.33 mg·g<sup>-1</sup>, respectively, at a natural pH value of 4.8, and the adsorption capacities of MB were 62.90, 179.78, and 220.49 mg·g<sup>-1</sup> at a pH of 12.00. Thus, both the MB adsorption removal rate and adsorption capacities were increased with the increase of pH value.

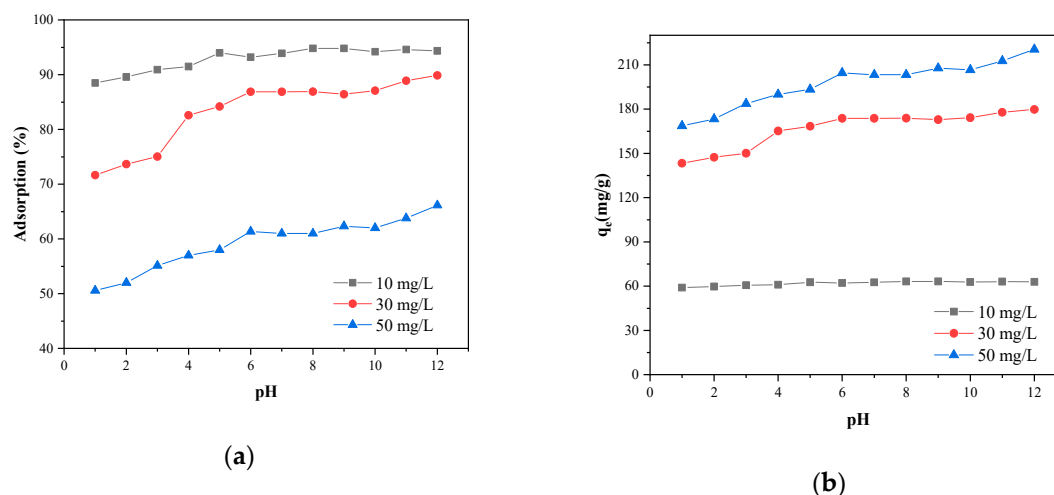


**Figure 5.** The adsorption rate (a) and the adsorption capacity ( $q_e$ ) (b) of MB adsorption on the SLS-C sample at various pH values ( $S/L = 0.15 \text{ g}\cdot\text{L}^{-1}$ , contact time = 120 min,  $25^\circ\text{C}$ ).

The pH values of dye solution control the extent of ionization of the acidic and basic compounds and affect the surface charge of SLS-C [7,33]. At lower pH, the dissociation of hydrogen ions ( $\text{H}^+$ ) by oxygen-containing functional groups on SLS-C would be inhibited, and the electronegativity of SLS-C and electrostatic attraction force between dye cation and SLS-C were relatively weak. Moreover, the fact that the free hydrogen ions inhibited the adsorption reaction of dye cation onto AC site by competing adsorption could lead to a reduction in MB removal rate. The increase in the concentration of hydroxide ions in the solution made the dissociation degree of MB small, and thus the removal rate of MB was improved as the pH value increased [34]. In addition, the dissociation degree of  $\text{H}^+$  by the oxygen-containing functional groups on the surface of the SLS-C increased with the increase of pH, which increased the electronegativity of SLS-C and the electrostatic attractive force between the dye cation and SLS-C [25]. Furthermore, hydroxyl groups (O-H) and carbonyl groups (C=O) on the surface of the adsorbent can also attract the cationic dye molecules under the condition of high pH value [35]. Therefore, SLS-C has a good adsorption capacity of MB in an alkaline environment.

The results have resemblance to previous studies by Karaca [11]. The study by Yagub et al. [36] showed that the adsorption rate of cationic dye MB by raw pine leaf biochar at high pH values was better than that at low pH values. The adsorption rate had a noticeable increase at pH from 2 to 7, and slightly increased at the range of pH 7–9. The effect of pH on MB adsorption by various ACs was studied by Kannan N et al. [37], showing that the adsorption capacity of dye increased with the increase of initial pH.

Figure 6 shows the zeta potential variation of AC with pH before and after modification. The  $\text{pH}_{\text{PZC}}$  of SLS-C and Virgin-C were 3.37 and 4.10. The result demonstrated that SLS-C has a higher surface electronegativity than that of Virgin-C, which was attribute to the hydrophobic alkyl end of surfactant attached to the nonpolar surface of activated carbon by van der Waals force. The AC surface oxygen-containing functional groups such as carboxyl and phenolic hydroxyl were covered with SLS to lead the amount of dissociated  $\text{H}^+$  to decrease. The enhanced electronegativity of SLS-C made it have a better electrostatic attraction and adsorption capacity to MB than Virgin-C. When pH was around 4 to 8, the adsorption rate of MB on SLS-C was relatively stable in this experiment. Therefore, a pH value of 5 was chosen for the adsorption research.

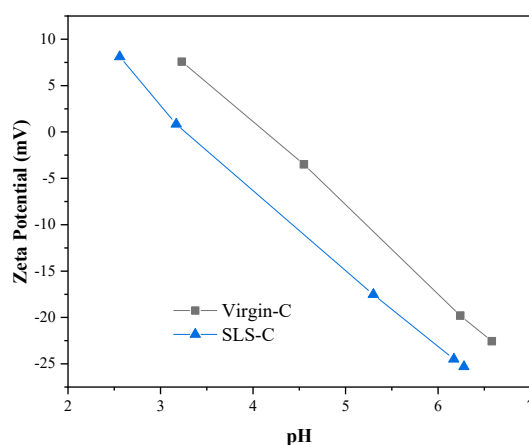


Figure 6. The zeta potential of Virgin-C and SLS-C.

#### 3.4. Effect of Adsorbent Dose

Adsorbent dose is an important factor that affects the adsorption performance. The influence of adsorbent dose in adsorption of MB was studied to obtain a most appropriate amount of adsorbent at various MB concentrations [38]. The effect of adsorbent dose was studied by 100 mL of three different MB concentrations (10, 30, and 50 mg·L<sup>-1</sup>) under different adsorbent doses (5, 7.5, 10, 15, 20, 30, 40, 50, 75, and 100 mg), as shown in the diagram below (Figure 7). A similar trend in adsorption behavior of MB on SLS-C under various MB concentrations was observed.

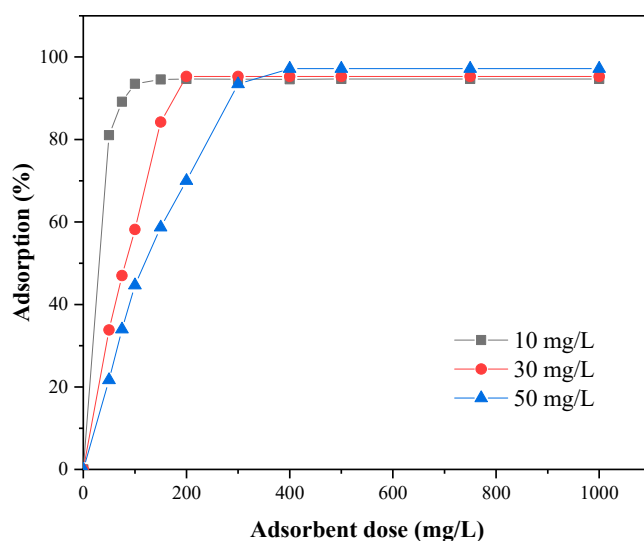
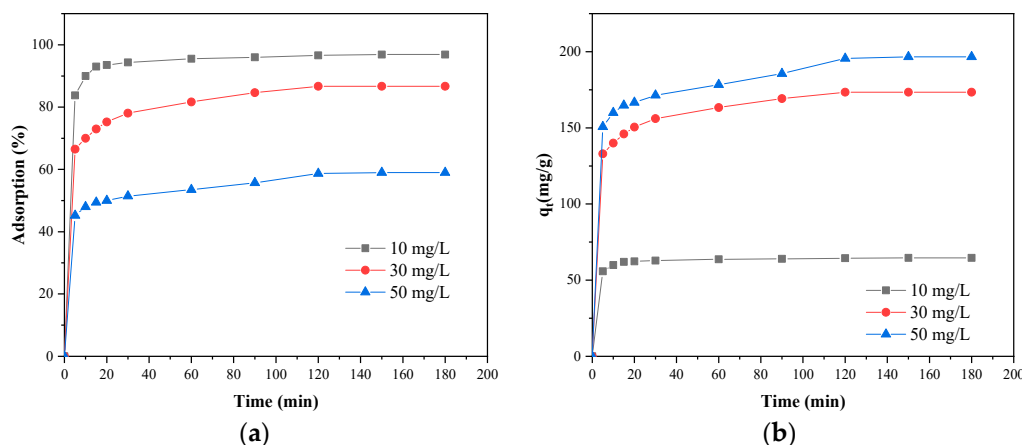


Figure 7. Effect of adsorbent dose on MB adsorption on SLS-C sample (contact time = 120 min).

As the mass of adsorbents increased, the removal rate of MB gradually increased due to the increases of the number of adsorbent pores and adsorption sites. The adsorption would tend to an equilibrium when the mass of adsorbent reached a certain value. The removal rate of MB reached the saturated value at adsorbent mass of 15, 20, and 30 mg corresponding to the initial MB concentration of 10, 30, and 50 mg·L<sup>-1</sup>, respectively. At high adsorbent dosages, the available number of MB dye molecules in solution was not enough to completely combine with all effective adsorption sites on the adsorbent, resulting in a surface equilibrium state and a reduction in the adsorption capacity per unit mass of adsorbent.

### 3.5. Effects of Contact Time

Figure 8 showed the relationship between the adsorption rate and the adsorption capacity of MB on SLS-C and time at three initial MB concentrations (10, 30, and 50 mg·L<sup>-1</sup>).



**Figure 8.** Effect of contact time on adsorption of MB on SLS-C at pH = 5.0, S/L = 0.15 g·L<sup>-1</sup>. (a) The adsorption rate; (b) the adsorption capacity.

It can be seen in Figure 8 that the removal efficiency and adsorption capacity of MB by SLS-C was increased with an increase in contact time and then reached a maximum value. The process was divided into two phases. The first step took 5–30 min to reach the relative adsorption equilibrium state called fast adsorption. This performance was due to the binding process between MB dye and the adsorption active sites, and functional groups on the SLS-C adsorbent were fully and efficiently completed. The absorption rate of the dye was controlled by the rate of the dye transported from the solution to the surface of the adsorbent particles. The second step was called slow adsorption process. After 30 min of contact time, the relative increase in the removal extent of MB was not significant, and with the increase of time, the adsorption rate decreased and gradually stabilized. This performance was due to the binding process between MB dye and the adsorption active sites, and functional groups on the SLS-C adsorbent were gradually saturated. The absorption rate of the dye was controlled by the rate of the dye transported from the exterior to the interior pore sites of the adsorbent particles [39].

Moreover, the lower the dye initial concentration, the shorter the time to achieve the adsorption equilibrium state. The results were basically consistent with previous studies on the removal rate of dyes [29]. Considering the relationship between the contact time and the MB removal, the contact time for subsequent experiments was selected as 120 min.

### 3.6. Effects of Initial MB Concentration

The influence of different initial dye concentrations (10, 20, 30, 40, 50 mg·L<sup>-1</sup>) on the decolorization efficiency of MB dye was studied using the same mass of SLS-C and adjusting the dye solution pH to 5. A 15 mg adsorbent sample was added to 100 mL dye solution and adsorbed for 120 min at 298K. The experimental data are given in Table 1.

According to the listed data (Table 1), the decolorization rate (%) of MB by 15 mg of the SLS-C adsorbent decreased from 96.6% to 58.7% when the initial dye concentration increased from 10 to 50 mg·L<sup>-1</sup>. However, as the initial dye concentration increased from 10 to 50 mg·L<sup>-1</sup>, the adsorption capacity at equilibrium ( $Q_e$ ) increased from 64.4 to 195.8 mg·g<sup>-1</sup>. Moreover, the maximum adsorption capacity at equilibrium ( $Q_e$ ) was calculated up to value of 195.8 mg·g<sup>-1</sup> when the dye concentration was 40 mg·L<sup>-1</sup>. It was found that when the MB concentration was greater than 40 mg·L<sup>-1</sup>, the adsorption sites on the adsorbent were completely adsorbed, and thus the adsorption amount of activated carbon at a MB concentration of 40 mg·L<sup>-1</sup> was similar to that at MB concentration of 50 mg·L<sup>-1</sup>.

**Table 1.** Effect of initial MB concentration on the percentage extraction of dye.

MB Concentration (mg·L <sup>-1</sup> )	SLS-C		Virgin-C	
	Percent Adsorption (%)	Adsorption Capacity (mg·g <sup>-1</sup> )	Percent Adsorption (%)	Adsorption Capacity (mg·g <sup>-1</sup> )
10	96.6	64.4	80.9	53.9
20	90.6	120.8	72.7	96.0
30	86.7	173.4	66.3	132.6
40	73.4	195.8	51.9	138.4
50	58.7	195.7	41.3	137.6

The removal extent of dyes was decreased with an increase in the initial MB concentration due to the lack of available active sites under high concentration condition of MB [40], whereas the adsorption capacity of MB on SLS-C increased with the increase of initial MB concentration. The sulfate functional group of SLS provided ion exchange sites conducive to the MB ion adsorption. Compared with untreated AC, activated carbon modified by anionic surfactant has more positively charged adsorption sites and high adsorptive capacity for removing cationic dye [12,27].

### 3.7. Adsorption Kinetics and Isotherm

#### 3.7.1. Adsorption Kinetics

Adsorption kinetics mainly studies the reaction rate between adsorbents and adsorbates and the factors affecting the reaction rate. The adsorption data were fitted by kinetic models and the adsorption mechanism was discussed according to the fitting results. The adsorption kinetics of MB on SLS-C were studied by using four kinetic equation models to confirm the most effective equation. The consistency between the experimental results and the theoretical values of the model was assessed on the basis of the coefficient of determination ( $R^2$  value was close to or equal to 1).

The principle of the pseudo-first-order kinetic model is that the reaction rate is proportional to the number of ions remaining in the solution, assuming that adsorption is controlled by diffusion steps [41]. It is assumed that the adsorption rate is proportional to the difference between the saturated concentration and the adsorption amount of SLS-C with time. The integral equation is shown below in Equation (6).

$$\ln(Q_e - Q_t) = \ln Q_e - k_1 t \quad (6)$$

where  $k_1$  is the rate constant of adsorption ( $\text{min}^{-1}$ ),  $Q_e$  is the quantity of dye adsorbed at equilibrium ( $\text{mg}\cdot\text{g}^{-1}$ ), and  $Q_t$  is the equilibrium concentration at various times  $t$  (in  $\text{mg}\cdot\text{L}^{-1}$ ). The rate constant in this model was determined by the slope of the plot of  $\ln(Q_e - Q_t)$  over time ( $t$ ). The results of  $R^2$  calculated were in the range of 0.644–0.974. In addition, the large differences between the value of  $Q_{e,exp}$  and  $Q_{e,cal}$  indicated that the pseudo-first order model was not an effective model to explain the adsorption process.

The pseudo-second-order kinetic model, which can be expressed as the reaction rate being proportional to the concentrations of the two reactants, assuming the adsorption is controlled by chemical adsorption steps, can be expressed by Equation (7) [42].

$$\frac{t}{Q_t} = \frac{1}{k_2 Q_e^2} + \frac{t}{Q_e} \quad (7)$$

where  $k_2$  is the second-order-rate constant ( $\text{g}\cdot\text{mg}^{-1}\cdot\text{min}^{-1}$ ) that can be determined for different MB concentrations according to the linear plots of  $t/Q_t$  versus  $t$ , as shown in Figure 9. The calculated correlation coefficients ( $R^2$ ) were found to be greater than 0.999, and the experimental  $Q_e$  differing from the calculated ones are listed in Table 2. Obviously, from the values calculated by pseudo-second-order

kinetic model,  $Q_{e,cal}$  had good agreement with the experimental  $Q_{e,exp}$ . This behavior indicated that the pseudo-second order model was the best model to explain the adsorption process of MB on SLS-C.

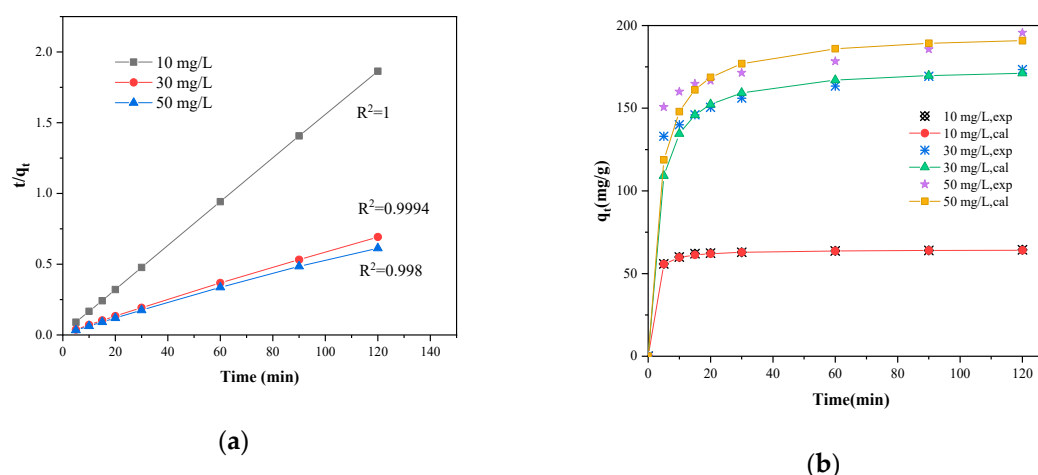


**Figure 9.** (a) Pseudo-second order plots and (b) the adsorption capacity ( $q_e$ ) for the adsorption of MB on SLS-C at various initial concentrations, pH = 5.0, S/L = 0.15 g·L<sup>-1</sup>, T = 25 °C.

**Table 2.** Pseudo-First-Order model and Pseudo-Second-Order model form removal of MB by SLS-C.

$C_0$ (mg·L <sup>-1</sup> )	$Q_{e,cal}$ (mg·g <sup>-1</sup> )	Pseudo-First-Order Model			Pseudo-Second-Order Model		
		$k_1$ (min <sup>-1</sup> )	$Q_e$ (mg·g <sup>-1</sup> ) (exp.)	$R^2$	$k_2$ (g·mg <sup>-1</sup> · min <sup>-1</sup> )	$Q_e$ (mg·g <sup>-1</sup> ) (exp.)	$R^2$
10	64.4	0.0090	4.4	0.644	0.00195	64.1	1
30	173.4	0.0107	40.9	0.966	0.00188	171.1	0.999
50	195.7	0.0069	42.1	0.974	0.00157	190.9	0.998

The intra-particle diffusion model divides the adsorption process into two main steps including the migration of solute molecules from aqueous solution to the surface of adsorbent particles and the diffusion of adsorbate molecules into the interior pores of the adsorbent [43].

The adsorption process was studied Weber–Morris intra-particle diffusion model which is expressed as Equation (8).

$$Q_t = k_{ip}t^{1/2} + C_i \quad (8)$$

where  $k_{ip}$  (mg·g<sup>-1</sup>·min<sup>-1/2</sup>) is the rate constant of the intra-particle diffusion model, and  $C_i$  is the constants related to boundary layer thickness expressed in milligrams per gram (mg·g<sup>-1</sup>), which can be calculated according to slope and intercept of the plot of  $Q_t$  versus the square root of time  $t^{1/2}$ .

The straight line fitted by the intra-particle model (as shown in Figure S2) without passing through the origin indicated that the adsorption process was controlled not only by the intra-particle diffusion but also by other adsorption processes. The constant  $C_i$  (57.64, 127.73, 144.74) was found to increase with the increase of MB dye concentration, which may have been due to the increase of the boundary layer thickness (as shown in Table 3). The high values of  $C_i$  indicated that the external diffusion of MB molecule on SLS-C was very important in the initial adsorption period. The values of  $R^2$  were close to 1 and show a good application of the intra-particle model in the sorption process.

**Table 3.** Intra-particle diffusion model and Elovich model from removal of MB by SLS-C.

$C_0$ ( $\text{mg}\cdot\text{L}^{-1}$ )	Intra-Particle Diffusion Model			Elovich Model		
	$k_{ip}$ ( $\text{mg}\cdot\text{g}^{-1}\cdot\text{min}^{-1/2}$ )	$C_i$	$R^2$	$\alpha$ ( $\text{mg}\cdot\text{g}^{-1}\cdot\text{min}^{-1}$ )	$\beta$ ( $\text{mg}\cdot\text{g}^{-1}$ )	$R^2$
10	$K_{ip1} = 3.800$ $K_{ip2} = 0.303$	57.64	0.985 0.974	2.395	0.436	0.816
30	4.426	127.73	0.957	14.373	0.078	0.997
50	4.542	144.74	0.974	14.197	0.078	0.970

The Elovich model of adsorption process was expressed as Equation (9), which describes adsorption in a non-ideal state. The adsorption process is divided into the fast adsorption and slow adsorption process.

$$Q_t = \frac{1}{\beta} \ln \alpha \beta + \frac{1}{\beta} \ln t \quad (9)$$

where  $\alpha$  represents the initial adsorption rate ( $\text{mg}\cdot\text{g}^{-1}\cdot\text{min}^{-1}$ ) and  $\beta$  is the desorption coefficient ( $\text{mg}\cdot\text{g}^{-1}$ ). The graph of  $Q_t$  versus  $\ln t$  is a line with a slope of  $1/\beta$  and an intercept of  $1/\beta \ln(\alpha \beta)$ . The correlation coefficient ( $R^2$ ) at MB concentrations of 10, 30, and 50  $\text{mg}\cdot\text{L}^{-1}$  were identified as being 0.816, 0.997, and 0.970, respectively. The fitting data calculated from Elovich kinetic model showed that when the initial concentration of MB was 10  $\text{mg}\cdot\text{L}^{-1}$ , the models described the observations not well. Nevertheless, that the experimental results could be well described by the Elovich model at the initial concentration of MB higher than 10  $\text{mg}\cdot\text{L}^{-1}$  indicated that the rate-limiting step was the intraparticle diffusion process but not the only process [22,44].

The results showed that the pseudo-second-order kinetic model can be used to describe the adsorption of MB on SLS-C and proved that chemical adsorption dominated the adsorption process. The adsorption process not only included the processes of the liquid film diffusion and the internal diffusion of micropores, but also the chemical adsorption process with electrons shared and gained or loss of electrons between cationic dyes and functional groups on the SLS-C surface [30].

### 3.7.2. Adsorption Isotherm

The adsorption process is divided into two parts, adsorbent adsorption pollutants and pollutants desorption from the adsorbent. When the rate of the two processes is the same, the adsorption will enter a dynamic equilibrium state. Adsorption isotherms are used to study the relationship between the equilibrium adsorption capacity and the equilibrium concentration of pollutants under certain conditions (temperature and pH remain unchanged). The adsorption isotherms were studied to provide a basis for revealing adsorption behavior, indicating possible adsorption mechanism, and estimating adsorption capacity. Three models, the Langmuir model, Freundlich model, and Temkin model, were used to describe adsorption isothermal behavior.

The Langmuir model assumes that adsorption is localized on a monolayer, and all adsorption sites on the adsorbent are homogeneous and have the same adsorption capacity [45]. The Langmuir isotherm equation is Equation (10):

$$\frac{C_e}{Q_e} = \frac{1}{Q_{max} K_L} + \frac{C_e}{Q_{max}} \quad (10)$$

where  $C_e$  is the equilibrium concentration ( $\text{mg}\cdot\text{L}^{-1}$ ),  $Q_e$  is the amount of adsorbed dye at equilibrium ( $\text{mg}\cdot\text{g}^{-1}$ ),  $Q_{max}$  ( $\text{mg}\cdot\text{g}^{-1}$ ) is the Langmuir constants that are related to the adsorption capacity, and  $K_L$  ( $\text{L}\cdot\text{mg}^{-1}$ ) is the adsorption rate. The value of  $R^2$  obtained from the linear graph of  $C_e/Q_e$  versus  $C_e$  was 0.993, which demonstrated that the adsorption process meets the Langmuir isotherm model, as exhibited in the diagram (Figure 10). The value of  $Q_{max}$  and  $K_L$  are shown in Table 4.

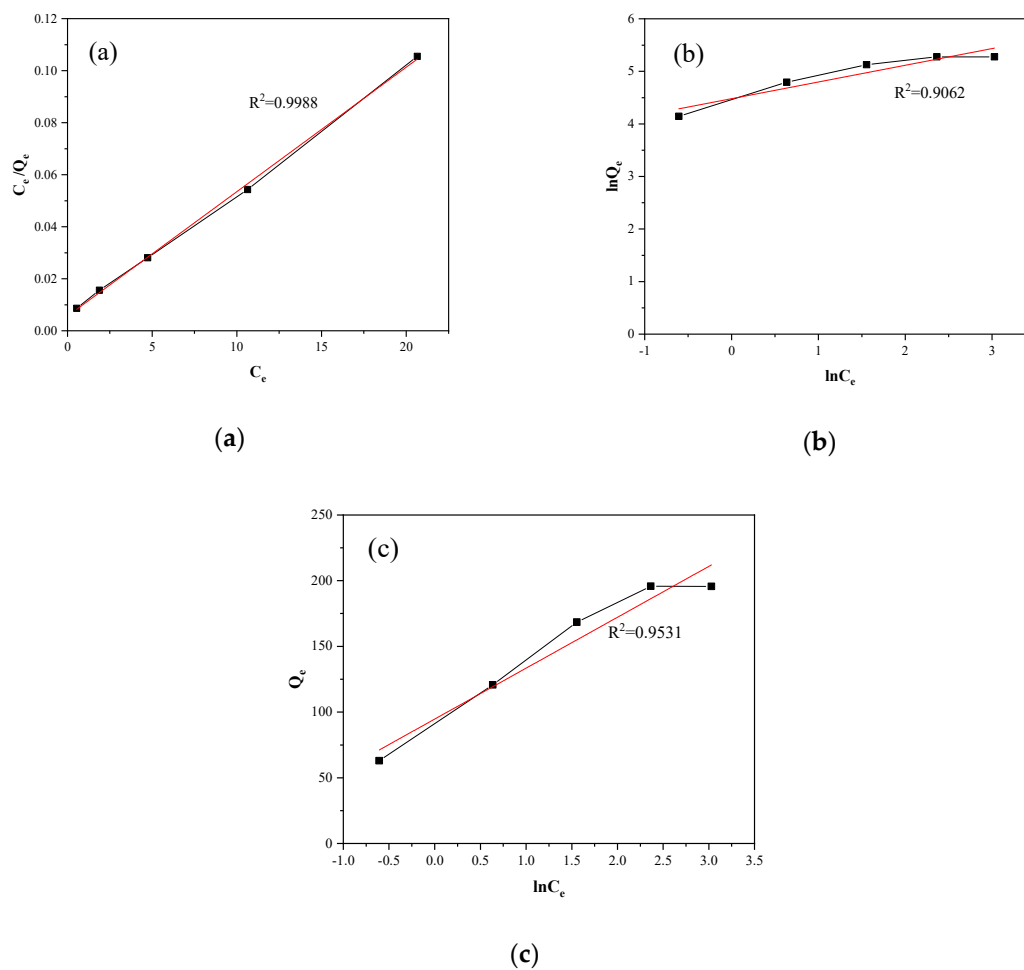


**Figure 10.** (a) Langmuir, (b) Freundlich, and (c) Temkin isotherm plots for adsorption of MB on SLS-C.

**Table 4.** Isotherm parameters of the Langmuir, Freundlich, and Temkin models.

Adsorption Model	Isotherm Parameters	$R^2$
Langmuir	$Q_{max} = 232.5 \text{ mg}\cdot\text{g}^{-1}$ $K_L = 0.842 \text{ L}\cdot\text{m}^{-1}\cdot\text{g}^{-1}$ $R_L = 0.106$	0.999
Freundlich	$K_f = 88.235 \text{ mg}\cdot\text{g}^{-1}$ $1/n = 0.318$	0.906
Temkin	$B = 38.73 \text{ J}\cdot\text{mol}^{-1}$ $A = 11.53 \text{ L}\cdot\text{g}^{-1}$ $b = 63.98 \text{ L}\cdot\text{g}^{-1}$	0.953

The feasibility of adsorbent adsorption was evaluated by  $R_L$ . It can be defined by Equation (11) [46]:

$$R_L = \frac{1}{1 + K_L C_0} \quad (11)$$

where  $C_0$  ( $\text{mg}\cdot\text{L}^{-1}$ ) is initial dye concentration. The value of  $R_L$  indicates the type of the isotherm: irreversible ( $R_L = 0$ ), favorable ( $0 < R_L < 1$ ), linear ( $R_L = 1$ ), or unfavorable ( $R_L > 1$ ). The  $R_L$  value of MB adsorption on SLS-C was in the range of 0.661–0.842. It can be testified that the adsorption process was favorable.

The Freundlich isotherm model is based on the assumption that multi-layer adsorption processes occur on heterogeneous surfaces. The Freundlich isotherm linear equation is shown in Equation (12):

$$\ln Q_e = \ln K_f + \frac{1}{n} \ln C_e \quad (12)$$

where  $K_f$  ( $\text{mg}\cdot\text{g}^{-1}$ ) is a constant related to the adsorption energy. The value of  $R^2$  obtained from the linear graph of  $\ln Q_e$  versus  $\ln C_e$  was 0.906. Compared the values of  $R^2$  of two isotherms models, the Langmuir model was more suitable for the experimental equilibrium adsorption data than the Freundlich model, as shown in Figure 10. The values of  $1/n$  and  $K_f$  were calculated and listed in Table 4. The slope ( $1/n$ ) values reflected adsorption intensity or surface heterogeneity. It is generally considered as a sign of a good adsorption process when the value of  $1/n$  is in the range of 0.1 to 1.0. In this experiment, the index value was within the range, indicating that the adsorption process was favorable. This was in line with the conclusion of the Langmuir model.

The Temkin model considers the interaction between adsorbent and contaminant as a chemical adsorption process. The Temkin isotherm equation are shown in Equations (13) and (14):

$$Q_e = \frac{RT}{b} \ln A + \frac{RT}{b} \ln C_e \quad (13)$$

$$B = \frac{RT}{b} \quad (14)$$

where  $b$  ( $\text{mg}\cdot\text{L}^{-1}$ ) is the Temkin isotherm constant,  $A$  ( $\text{L}\cdot\text{g}^{-1}$ ) is the Temkin isotherm equilibrium binding constant, and  $B$  is the constant related to the heat of adsorption ( $\text{J}\cdot\text{mol}^{-1}$ ). The calculated values of  $A$ ,  $B$ , and  $b$  are shown in Table 4.

The isotherm data were linearized using the Langmuir equation, as shown in Figure 10. The parameters of Langmuir isotherm are shown in Table 4. The high value of  $R^2$  indicated that there was a good agreement between the model parameters. The theoretical maximum adsorption capacity of MB on SLS-C, obtained by the Langmuir adsorption isothermal equation fitting, was up to  $232.5 \text{ mg}\cdot\text{g}^{-1}$ , whereas the theoretical maximum adsorption capacity of Virgin-C was  $153.8 \text{ mg}\cdot\text{g}^{-1}$ . The Freundlich equation and Temkin equation were also used to fit the same data, as shown in Figure 10. The relevant coefficients can be calculated from three isotherms, such as  $K_L$ ,  $Q_{max}$ ,  $R_L$ ,  $K_f$ ,  $n$ ,  $A$ ,  $B$ , and  $b$ . The values are listed in Table 4.

The adsorption isotherm analysis results were in good agreement with the Langmuir, Freundlich, and Temkin models, but the Langmuir model had better consistency. These results indicated that the MB adsorption sites of the adsorbent were homogeneous, which was consistent with the assumption of the Langmuir model. For SLS-C, the surfactant molecules covered the AC surface uniformly, resulting in the homogeneous adsorption sites. Therefore, it can be inferred that the adsorption mechanism of MB adsorption by SLS-C was the physical and chemical monolayer adsorption.

### 3.8. Temperature Effect and Thermodynamic Parameters

The influence of temperature was studied by three MB concentrations (10, 30, and  $50 \text{ mg}\cdot\text{L}^{-1}$ ) at different temperature values (25, 35, 45, and  $55^\circ\text{C}$ ) and the results are graphed in Figure 11. The higher the temperature, the higher the adsorption ability of MB on SLS-C at all concentrations. This indicated that the adsorption was a spontaneous endothermic process.

The thermal motion, the solubility, and the chemical potential of dye molecules increased with the increase of temperature [47]. Moreover, the pore structure of AC was closely related to temperature. The pore structure and number of active adsorption sites of AC increased with the increase of temperature due to thermal expansion. These reasons led to the increase of adsorption capacity of MB on SLS-C with the increase of temperature.

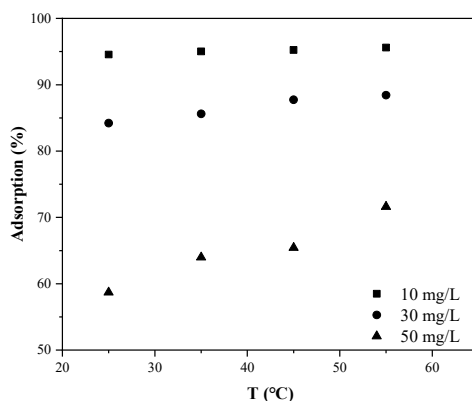


**Figure 11.** Influence of temperature on MB removal efficiency by SLS-C (adsorbent dosage S/L = 0.15 g·L<sup>-1</sup>, pH = 5.0, contact time = 120 min).

The temperature effect and sorption mechanism were further discussed in the study of adsorption thermodynamics. The thermodynamics of adsorption of SLS-C were analyzed from the view of energy. Studying on the driving force of adsorption by the adsorption thermodynamics method determined whether the adsorption process was spontaneous or not. The values of thermodynamic parameters, such as free energy change ( $\Delta G$ ), enthalpy change ( $\Delta H$ ), and entropy change ( $\Delta S$ ), are usually calculated on the basis of the thermodynamic formulas shown in Equations (15)–(18) [48]:

$$\Delta G = -RT \ln K_C, \quad (15)$$

$$K_C = \frac{Q_e}{C_e}, \quad (16)$$

$$\ln K_C = \frac{\Delta S}{R} - \frac{\Delta H}{RT} \quad (17)$$

$$\Delta G = \Delta H - T\Delta S \quad (18)$$

where  $K_C$  is the thermodynamic constant,  $R$  is the universal gas constant (8.314 J·mol<sup>-1</sup>·K<sup>-1</sup>), and  $T$  is the absolute temperature (K). The  $\Delta G$  is the Gibbs free energy change (kJ·mol<sup>-1</sup>),  $\Delta S$  is the entropy change (kJ·mol<sup>-1</sup>·K<sup>-1</sup>), and  $\Delta H$  is the enthalpy change (kJ·mol<sup>-1</sup>). The slope and intercept of the linear graph about  $\ln K_C$  versus  $1/T$ , as shown in Figure 12, can be respectively obtained from the values of  $\Delta H$  and  $\Delta S$ , as listed in Table 5.

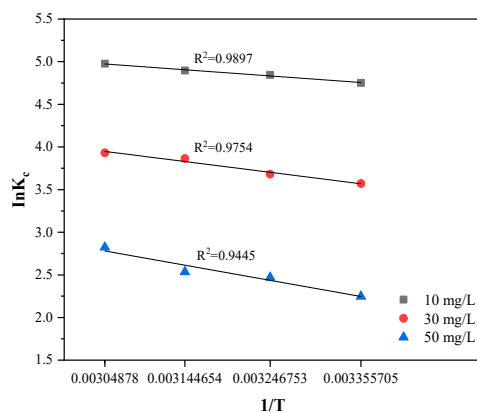


**Figure 12.** Thermodynamics parameters on the adsorption of MB by SLS-C.

**Table 5.** Thermodynamic parameters for removal efficiency of MB on SLS-C.

Thermodynamics				
c/mg·L <sup>-1</sup>	T/K	ΔG/kJ·mol <sup>-1</sup>	ΔS/kJ·mol <sup>-1</sup> ·K <sup>-1</sup>	ΔH/kJ·mol <sup>-1</sup>
10	298	-11.78	0.059	5.90
	308	-12.38		
	318	-12.97		
	328	-13.56		
30	298	-8.84	0.064	10.28
	308	-9.48		
	318	-10.12		
	328	-10.77		
50	298	-5.57	0.067	14.46
	308	-6.24		
	318	-6.91		
	328	-7.58		

The negative  $\Delta G$  values, which can be seen from Table 5, demonstrated the discolored process of MB on SLS-C in terms of feasibility and spontaneity [49]. The positive  $\Delta H$  values of 5.90, 10.28, and 14.46  $\text{kJ}\cdot\text{mol}^{-1}$  at different temperatures prove that the adsorption was an endothermic process at initial dye concentrations of 10  $\text{mg}\cdot\text{L}^{-1}$ , 30  $\text{mg}\cdot\text{L}^{-1}$ , 50  $\text{mg}\cdot\text{L}^{-1}$ , respectively [50]. In the adsorption of different MB dye concentrations on SLS-C,  $\Delta S$  values were 0.059, 0.064, and 0.067  $\text{kJ}\cdot\text{mol}^{-1}\cdot\text{K}^{-1}$ , respectively. The positive values of  $\Delta S$  indicated that the randomness of the solid/solution interface increased during the adsorption process [13].

### 3.9. Effect of Additive Salts

The effects of different salts such as NaCl, KCl, CaCl<sub>2</sub>, NH<sub>4</sub>Cl, MgSO<sub>4</sub>·7H<sub>2</sub>O, NaNO<sub>2</sub>, and FeSO<sub>4</sub> on adsorption were studied in 100.0 mL MB solution under the different concentration conditions of 10, 30, and 50  $\text{mg}\cdot\text{L}^{-1}$ . A total of 200.0 mg of additive salt was added into the dye solution, adjusting the pH value to 5.0 and oscillating for 30 min. The effect of salt species on the adsorption of MB on SLS-C are listed in Table 6.

**Table 6.** Effect of salt species on the removal efficiency (%) of MB at 25°C, t = 30 min.

MB Concentration (mg·L <sup>-1</sup> )	Removal Efficiency (%) in Presence of Salt Species							
	None	NaCl	KCl	CaCl <sub>2</sub>	NH <sub>4</sub> Cl	MgSO <sub>4</sub>	NaNO <sub>2</sub>	FeSO <sub>4</sub>
10	94.3	94.6	94.6	94.6	94.6	94.6	94.6	90.4
30	78.1	79.7	77.0	78.3	78.3	73.7	85.3	60.5
50	53.2	55.5	52.7	53.9	53.9	52.0	56.9	44.2

The presence of coexisting ions (Na<sup>+</sup>, K<sup>+</sup>, Ca<sup>2+</sup>, NH<sub>4</sub><sup>+</sup>, Mg<sup>2+</sup>) had little effect on the adsorption of MB on SLS-C. When the concentration of MB was 30  $\text{mg}\cdot\text{L}^{-1}$ , the removal rates of MB in the presence of coexisting ions were 73.7%-79.7%, which was similar to the removal rates of 78.1% in the absence of ions. When the dye concentration was 50  $\text{mg}\cdot\text{L}^{-1}$ , the removal rate of MB in the presence of coexisting ions (52.0%-55.5%) was similar to that in the absence of ions (53.2%). This result is similar to the study on effect of the cations (Na<sup>+</sup>, K<sup>+</sup>, Ca<sup>2+</sup>) on adsorption of ammonium on SLS-C by Wooram Lee [27]. It indicated that the adsorption process was as insensitive to ionic as Na<sup>+</sup>, K<sup>+</sup>, Ca<sup>2+</sup>, NH<sub>4</sub><sup>+</sup>, and Mg<sup>2+</sup> [51].

The adsorption capacity of MB on SLS-C increased slightly when NaCl, CaCl<sub>2</sub>, or NH<sub>4</sub>Cl were present in the solution system. It may have been due to the increase of dimerization reaction of MB in solution in the presence of forces such as ion dipole, dipole-dipole interaction, and van-der-Waals force among dye molecules. The result agreed well with the article of Mohamed E. Mahmoud

that additive salts (NaCl, NaAc, KCl, MgSO<sub>4</sub>, NH<sub>4</sub>Cl, and CaCl<sub>2</sub>) improve the removal rate of dye by surfactant-modified AC [22]. When the ion (NO<sup>2-</sup>) was present, it had a greater impact on the adsorption of MB by SLS-C. When MB concentration was 30 mg·L<sup>-1</sup>, the removal rate of MB (85.3%) in the presence of coexisting ions (NO<sup>2-</sup>) was higher than that in the absence of ions (78.1%). The reason may be that NO<sup>2-</sup> has strong oxidation capacity in dilute solutions. Nitrite such as sodium nitrite and potassium nitrate are widely used in dye production. At a MB concentration of 50 mg·L<sup>-1</sup>, the removal rate of MB (44.2%) by SLS-C in the presence of competitive cation (Fe<sup>2+</sup>) was lower than that in the absence of ions (53.2%). The rate of adsorption was reduced because the strong reducibility ferrous ions occupied the adsorption site of MB on SLS-C.

### 3.10. Decolorization of MB in Real Water Samples by SLS-C

The adsorption rate of MB by SLS-C in three different real water samples of tap water, raw water, and waste samples are listed in Table 7. The tap water sample was collected from laboratory faucets, raw water sample was collected from the back of the Pearl River, and waste water sample was collected from a nameless river in the campus. The parameters of the water samples are shown in Table S1. A certain amount of MB was added into 100.0 mL water samples and prepared at concentrations of 10.0, 30.0, and 50.0 mg·L<sup>-1</sup>, respectively. All the samples were adjusted to pH of 5.0 and shaken for 30min in a shaker. Distilled water samples were treated as blank water samples for comparison. The experimental results expressed that the adsorption rate of MB by SLS-C in real water samples was slightly improved relative to modeling dye wastewater.

**Table 7.** Adsorptive removal of MB dye from real water samples' SLS-C adsorbent.

Water Sample	MB Concentration (mg·L <sup>-1</sup> )	Removal (%)
Distilled water	10	94.3
	30	78.1
	50	53.4
Tap water	10	94.3
	30	80.1
	50	54.1
Raw water	10	94.3
	30	81.0
	50	55.3
waste water	10	94.3
	30	81.1
	50	55.9

## 4. Conclusions

This study showed that AC modified by anionic surfactants could significantly improve the adsorption properties of MB on AC. The solution initial pH, adsorbent dosage, contact time, initial MB concentration, temperature, and additive salts had a great impact on adsorption properties. The high adsorption capacity of SLS-C can be attributed to the hydrophobic group of the surfactant, which is expected to bind to the hydrophobic surface of AC. A specific binding site with the anionic functional group on SLS-C provided an efficient sorption field for the MB target dye cations. The SLS-C has advantages such as a strong affinity of acid conjugate base, a number of functional groups per unit mass adsorbent, and good dispersibility. The study of adsorption of dyes in aqueous solutions at pH values in the range of 1.0–12.0 confirmed that the adsorption rate increased with the increase of pH. The adsorption rate of MB by SLS-C increased with increased temperature. The adsorption kinetics conformed to the pseudo-second-order reaction model and the adsorption isotherm conformed to the Langmuir adsorption isotherm. The negative  $\Delta G$  values and positive  $\Delta H$  values proved that the adsorption process was an endothermic and spontaneous process. The theoretical maximum

adsorption capacity of MB on SLS-C was  $232.5 \text{ mg}\cdot\text{g}^{-1}$ , whereas the theoretical maximum adsorption capacity of Virgin-C was  $153.8 \text{ mg}\cdot\text{g}^{-1}$ . The adsorption equilibrium time was about 120 min. The presence of cations such as  $\text{Na}^+$ ,  $\text{K}^+$ ,  $\text{Ca}^{2+}$ ,  $\text{NH}_4^+$ , and  $\text{Mg}^{2+}$  had negligible impact on the adsorption of MB on SLS-C (< 5%). The adsorption capacity was significantly improved in the presence of  $\text{NO}_2^-$  and decreased in the presence of cation  $\text{Fe}^{2+}$ . The application of SLS-C in the decolorization of MB in tap water, raw water, and waste water proved that the existence of ions has little influence in the MB adsorption in real water samples.

**Supplementary Materials:** The following are available online at <http://www.mdpi.com/2073-4441/12/2/587/s1>, Figure S1: title, Table S1: title, Video S1: title. Figure S1: MB standard curve (at pH of 5). Figure S2: The intraparticle diffusion model plots for the adsorption of MB on SLS-C (a) at MB concentration of 10 mg/L, and (b) at MB concentrations of 10, 30, and 50 mg/L. Table S1: The water quality parameters of different water samples.

**Author Contributions:** Y.K. conceived the study. She also conducted the experiment, data collection, and analysis of data, and prepared the first edition of the manuscript. X.Z. participated in the design of the study and helped to draft and edit the manuscript. S.Z. helped to edit the manuscript. All authors read and approved the final manuscript.

**Funding:** This research was funded by National Key R&D Plan Project of China (2016YFC0400702-2), and the Research Funds for the National Natural Science Foundation (no. 21377041).

**Conflicts of Interest:** The authors declare no conflict of interest.

## References

1. Wong, Y.C.; Szeto, Y.S.; Cheung, W.H.; McKay, G. Adsorption of acid dyes on chitosan—equilibrium isotherm analyses. *Process. Biochem.* **2004**, *39*, 695–704. [[CrossRef](#)]
2. Tan, I.A.W.; Ahmad, A.L.; Hameed, B.H. Adsorption of basic dye on high-surface area activated carbon prepared from coconut husk: Equilibrium, kinetic and thermodynamic studies. *J. Hazard. Mater.* **2008**, *154*, 337–346. [[CrossRef](#)]
3. Pavithra, K.G.; Kumar, P.S.; Jaikumar, V.; Rajan, P.S. Removal of colorants from wastewater: A review on sources and treatment strategies. *J. Ind. Eng. Chem.* **2019**, *75*, 1–19. [[CrossRef](#)]
4. Verma, A.K.; Dash, R.R.; Bhunia, P. A review on chemical coagulation/flocculation technologies for removal of colour from textile wastewaters. *J. Environ. Manag.* **2012**, *93*, 154–168. [[CrossRef](#)] [[PubMed](#)]
5. Yu, S.; Liu, M.; Ma, M.; Qi, M.; Lü, Z.; Gao, C. Impacts of membrane properties on reactive dye removal from dye/salt mixtures by asymmetric cellulose acetate and composite polyamide nanofiltration membranes. *J. Membr. Sci.* **2010**, *350*, 83–91. [[CrossRef](#)]
6. Alventosa-deLara, E.; Barredo-Damas, S.; Alcaina-Miranda, M.I.; Iborra-Clar, M.I. Ultrafiltration technology with a ceramic membrane for reactive dye removal: Optimization of membrane performance. *J. Hazard. Mater.* **2012**, *209–210*, 492–500. [[CrossRef](#)] [[PubMed](#)]
7. Asghar, A.; Abdul Raman, A.A.; Wan Daud, W.M.A. Advanced oxidation processes for in-situ production of hydrogen peroxide/hydroxyl radical for textile wastewater treatment: A review. *J. Clean. Prod.* **2015**, *87*, 826–838. [[CrossRef](#)]
8. Kordouli, E.; Bourikas, K.; Lycourghiotis, A.; Kordulis, C. The mechanism of azo-dyes adsorption on the titanium dioxide surface and their photocatalytic degradation over samples with various anatase/rutile ratios. *Catal. Today* **2015**, *252*, 128–135. [[CrossRef](#)]
9. Yagub, M.T.; Sen, T.K.; Afroz, S.; Ang, H.M. Dye and its removal from aqueous solution by adsorption: A review. *Adv. Colloid Interface Sci.* **2014**, *209*, 172–184. [[CrossRef](#)]
10. Sun, D.; Zhang, X.; Wu, Y.; Liu, X. Adsorption of anionic dyes from aqueous solution on fly ash. *J. Hazard. Mater.* **2010**, *181*, 335–342. [[CrossRef](#)]
11. Karaca, S.; Gürses, A.; Açıkyıldız, M.; Ejder, M.K. Adsorption of cationic dye from aqueous solutions by activated carbon. *Microporous Mesoporous Mater.* **2008**, *115*, 376–382. [[CrossRef](#)]
12. Xiang, Y.; Gao, M.; Shen, T.; Cao, G.; Zhao, B.; Guo, S. Comparative study of three novel organo-clays modified with imidazolium-based gemini surfactant on adsorption for bromophenol blue. *J. Mol. Liquids* **2019**, *286*. [[CrossRef](#)]

13. Fan, S.; Wang, Y.; Wang, Z.; Tang, J.; Li, X. Removal of methylene blue from aqueous solution by sewage sludge-derived biochar: Adsorption kinetics, equilibrium, thermodynamics and mechanism. *J. Environ. Chem. Eng.* **2017**, *5*, 601–611. [[CrossRef](#)]
14. Wang, G.; Wang, S.; Sun, Z.; Zheng, S.; Xi, Y. Structures of nonionic surfactant modified montmorillonites and their enhanced adsorption capacities towards a cationic organic dye. *Appl. Clay Sci.* **2017**, *148*, 1–10. [[CrossRef](#)]
15. Wang, W.; Huang, G.; An, C.; Zhao, S.; Chen, X.; Zhang, P. Adsorption of anionic azo dyes from aqueous solution on cationic gemini surfactant-modified flax shives: Synchrotron infrared, optimization and modeling studies. *J. Clean. Prod.* **2018**, *172*, 1986–1997. [[CrossRef](#)]
16. Hailu, S.L.; Nair, B.U.; Mesfin, R.A.; Diaz, I.; Tessema, M. Preparation and characterization of cationic surfactant modified zeolite adsorbent material for adsorption of organic and inorganic industrial pollutants. *J. Environ. Chem. Eng.* **2017**, *5*, 3319–3329. [[CrossRef](#)]
17. Jiménez-Castañeda, M.; Medina, D. Use of Surfactant-Modified Zeolites and Clays for the Removal of Heavy Metals from Water. *Water* **2017**, *9*, 235. [[CrossRef](#)]
18. Leng, L.; Yuan, X.; Zeng, G.; Shao, J.; Chen, X.; Wu, Z.; Wang, H.; Peng, X. Surface characterization of rice husk bio-char produced by liquefaction and application for cationic dye (Malachite green) adsorption. *Fuel* **2015**, *155*, 77–85. [[CrossRef](#)]
19. Mohamed, M.M. Acid dye removal: Comparison of surfactant-modified mesoporous FSM-16 with activated carbon derived from rice husk. *J. Colloid Interface Sci.* **2004**, *272*, 28–34. [[CrossRef](#)]
20. Abdel-Fattah, T.M.; Mohamed, T.M.; Mahmoud, E.; Somia, B.; Matthew, A.; Huff, D.; James, W.L.; Sandeep, K. Biochar from woody biomass for removing metal contaminants and carbon sequestration. *J. Ind. Eng. Chem.* **2015**, *22*, 103–109. [[CrossRef](#)]
21. Mubarik, S.; Saeeda, A.; Athar, M.M.; Iqbal, M. Characterization and mechanism of the adsorptive removal of 2,4,6-trichlorophenol by biochar prepared from sugarcane baggase. *J. Ind. Eng. Chem.* **2016**, *33*, 115–121. [[CrossRef](#)]
22. Mahmoud, M.E.; Nabil, G.M.; El-Mallah, N.M.; Bassiouny, H.I.; Kumar, S.; Abdel-Fattah, T.M. Kinetics, isotherm and thermodynamic studies of the adsorption of reactive red 195 A dye from water by modified Switchgrass Biochar adsorbent. *J. Ind. Eng. Chem.* **2016**, *37*, 156–167. [[CrossRef](#)]
23. Pathania, D.; Sharma, S.; Singh, P. Removal of methylene blue by adsorption onto activated carbon developed from *Ficus carica* bast. *Arab. J. Chem.* **2017**, *10*, S1445–S1451. [[CrossRef](#)]
24. Rafatullah, M.; Sulaiman, O.; Hashim, R.; Ahmad, A. Adsorption of methylene blue on low-cost adsorbents: A review. *J. Hazard. Mater.* **2010**, *177*, 70–80. [[CrossRef](#)] [[PubMed](#)]
25. Zhang, R. Adsorption of Dye by Modified Activated Carbon and Heavy and Heavy Metals by Rice Husk-Based Activated Carbon. Master's Thesis, Nanjing Agricultural University, Nanjing, China, 2011. (In Chinese).
26. Choi, H.D.; Jung, W.S.; Cho, J.M.; Ryu, B.G.; Yang, J.S.; Baek, K. Adsorption of Cr(VI) onto cationic surfactant-modified activated carbon. *J. Hazard. Mater.* **2009**, *166*, 642–646. [[CrossRef](#)]
27. Lee, W.; Yoon, S.; Choe, J.K.; Lee, M.; Choi, Y. Anionic surfactant modification of activated carbon for enhancing adsorption of ammonium ion from aqueous solution. *Sci. Total Environ.* **2018**, *639*, 1432–1439. [[CrossRef](#)]
28. Lin, S.Y.; Chen, W.f.; Cheng, M.T.; Li, Q. Investigation of factors that affect cationic surfactant loading on activated carbon and perchlorate adsorption. *Colloids Surf. A Physicochem. Eng. Asp.* **2013**, *434*, 236–242. [[CrossRef](#)]
29. Choi, H.D.; Shin, M.C.; Kim, D.H.; Jeon, C.S.; Baek, K. Removal characteristics of reactive black 5 using surfactant-modified activated carbon. *Desalination* **2008**, *223*, 290–298. [[CrossRef](#)]
30. Namasivayam, C.; Suresh Kumar, M.V. Removal of chromium (VI) from water and wastewater using surfactant modified coconut coir pith as a biosorbent. *Bioresour. Technol.* **2008**, *99*, 2218–2225. [[CrossRef](#)]
31. Zhou, Y.; Wang, Z.; Andrew, H.; Ren, B. Gemini Surfactant-Modified Activated Carbon for Remediation of Hexavalent Chromium from Water. *Water* **2018**, *10*, 91. [[CrossRef](#)]
32. Akhter, M.S. Effect of acetamide on the critical micelle concentration of aqueous solutions of some surfactants. *Colloids Surf. A Physicochem. Eng. Asp.* **1997**, *121*, 103–109. [[CrossRef](#)]

33. Fu, J.; Chen, Z.; Wang, M.; Liu, S.; Zhang, J.; Zhang, J.; Han, R.; Xu, Q. Adsorption of methylene blue by a high-efficiency adsorbent (polydopamine microspheres): Kinetics, isotherm, thermodynamics and mechanism analysis. *Chem. Eng. J.* **2015**, *259*, 53–61. [[CrossRef](#)]
34. Wu, S.H.; Pendleton, P. Adsorption of anionic surfactant by activated carbon: Effect of surface chemistry, ionic strength, and hydrophobicity. *J. Colloid Interface Sci.* **2001**, *243*, 306–315. [[CrossRef](#)]
35. Wang, C. Fabrication of Polyacrylonitrile-Based Activated Carbon Fibers Functionalized Sodium Dodecyl Sulfate for the Adsorptive Removal of Organic Dye from Aqueous Solution. Master's Thesis, Hunan University, Changsha, China, 2017. (In Chinese).
36. Yagub, M.T.; Sen, T.K.; Ang, H.M. Equilibrium, Kinetics, and Thermodynamics of Methylene Blue Adsorption by Pine Tree Leaves. *Water Air Soil Pollut.* **2012**, *223*, 5267–5282. [[CrossRef](#)]
37. Kannan, N.; Sundaram, M.M. Kinetics and mechanism of removal of methylene blue by adsorption on various carbons—a comparative study. *Dye Pigment* **2001**, *51*, 25–40. [[CrossRef](#)]
38. Salleh, M.A.M.; Mahmoud, D.K.; Karim, W.A.; Idris, A. Cationic and anionic dye adsorption by agricultural solid wastes: A comprehensive review. *Desalination* **2011**, *280*, 1–13. [[CrossRef](#)]
39. Amin, N.K. Removal of reactive dye from aqueous solutions by adsorption onto activated carbons prepared from sugarcane bagasse pith. *Desalination* **2008**, *223*, 152–161. [[CrossRef](#)]
40. Eren, Z.; Acar, F.N. Adsorption of Reactive Black 5 from an aqueous solution: Equilibrium and kinetic studies. *Desalination* **2006**, *194*, 1–10. [[CrossRef](#)]
41. Plazinski, W.; Rudzinski, W.; Plazinska, A. Theoretical models of sorption kinetics including a surface reaction mechanism: A review. *Adv. Colloid Interface Sci.* **2009**, *152*, 2–13. [[CrossRef](#)]
42. Ho, Y.S.; McKay, G. Pseudo-second order model for sorption processes. *Process Biochem.* **1999**, *34*, 451–465. [[CrossRef](#)]
43. Feng, M.; You, W.; Wu, Z.; Chen, Q.; Zhan, H. Mildly alkaline preparation and methylene blue adsorption capacity of hierarchical flower-like sodium titanate. *ACS Appl. Mater. Interfaces* **2013**, *5*, 12654–12662. [[CrossRef](#)] [[PubMed](#)]
44. Huang, X.; Bu, H.; Jiang, G.; Zeng, M. Cross-linked succinyl chitosan as an adsorbent for the removal of Methylene Blue from aqueous solution. *Int. J. Biol. Macromol.* **2011**, *49*, 643–651. [[CrossRef](#)] [[PubMed](#)]
45. Mall, I.D.; Srivastava, V.C.; Agarwal, N.K. Removal of Orange-G and Methyl Violet dyes by adsorption onto bagasse fly ash—kinetic study and equilibrium isotherm analyses. *Dyes Pigment* **2006**, *69*, 210–223. [[CrossRef](#)]
46. Yao, Y.; Xu, F.; Chen, M.; Xu, Z.; Zhu, Z. Adsorption behavior of methylene blue on carbon nanotubes. *Bioresour. Technol.* **2010**, *101*, 3040–3046. [[CrossRef](#)]
47. Mouni, L.; Belkhir, L.; Bollinger, J.C.; Bouzaza, A.; Assadi, A.; Tirri, A.; Dahmoune, F.; Madani, K.; Reminie, H. Removal of Methylene Blue from aqueous solutions by adsorption on Kaolin: Kinetic and equilibrium studies. *Appl. Clay Sci.* **2018**, *153*, 38–45. [[CrossRef](#)]
48. Gobi, K.; Mashitah, M.D.; Vadivelu, V.M. Adsorptive removal of methylene blue using novel adsorbent from palm oil mill effluent waste activated sludge: Equilibrium, thermodynamics and kinetic studies. *Chem. Eng. J.* **2011**, *171*, 1246–1252. [[CrossRef](#)]
49. Auta, M.B.H. Hameed, Chitosan–clay composite as highly effective and low cost adsorbent for batch and fixed-bed adsorption of methylene blue. *Chem. Eng. J.* **2014**, *237*, 350–361. [[CrossRef](#)]
50. Bulut, Y.; Aydın, H. A kinetics and thermodynamics study of methylene blue adsorption on wheat shells. *Desalination* **2006**, *194*, 259–267. [[CrossRef](#)]
51. Que, W.; Jiang, L.H.; Wang, C.; Liu, Y.G.; Zeng, Z.W.; Wang, X.H.; Ning, Q.M.; Liu, S.H.; Zhang, P.; Liu, S.B. Influence of sodium dodecyl sulfate coating on adsorption of methylene blue by biochar from aqueous solution. *J. Environ. Sci.* **2018**, *70*, 166–174. [[CrossRef](#)]

